

# Interradical motion can push magnetosensing precision towards quantum limits

Luke D. Smith<sup>1,2</sup> <sup>1</sup>, Farhan T. Chowdhury<sup>1</sup> <sup>1</sup>, Jonas Glatthard<sup>3</sup> <sup>1</sup> and Daniel R. Kattnig<sup>1,2,\*</sup> <sup>1</sup>

<sup>1</sup>*Department of Physics, University of Exeter, Stocker Road, Exeter, Devon, EX4 4QL, United Kingdom.*

<sup>2</sup>*Living Systems Institute, University of Exeter, Stocker Road, Exeter, Devon, EX4 4QD, United Kingdom.*

<sup>3</sup>*School of Physics and Astronomy, University of Nottingham, Nottingham NG7 2RD, United Kingdom.*

(Dated: June 27, 2025)

Magnetosensitive spin-correlated radical-pairs (SCRPs) offer a promising platform for noise-robust quantum metrology. However, unavoidable interrational interactions, such as electron-electron dipolar and exchange couplings, alongside deleterious perturbations resulting from intrinsic radical motion, typically degrade their potential as magnetometers. In contrast to this, we show how structured molecular motion modulating interrational interactions in a *live* chemical sensor in cryptochrome can, in fact, increase sensitivity and, more so, push precision in estimating magnetic field directions closer to the quantum Cramér-Rao bound, suggesting near-optimal metrological performance. Remarkably, this approach to optimality is amplified under environmental noise and persists with increasing complexity of the spin system, suggesting that perturbations inherent to such natural systems have enabled them to operate closer to the quantum limit to more effectively extract information from the weak geomagnetic field. This insight opens the possibility of channeling the underlying physical principles of motion-induced modulation of electron spin-spin interactions towards devising efficient handles over emerging molecular quantum information technologies.

*Introduction.*—The sensitivity of spin-correlated radical-pairs (SCRPs) to weak magnetic fields presents exciting avenues for potential applications across quantum technologies and biophysics [1–7]. In a physiological context, SCRPs in the protein cryptochrome are widely considered candidate magnetoreceptors of a chemical compass sense for migratory navigation [8–11]. Such SCRPs function in noisy and complex condensed-phase regimes at ambient temperature while subjected to strong interrational interactions, such as electron-electron dipolar (EED) and exchange couplings, and environmentally induced structural fluctuations [12–15]. In engineered biradicals [16–19], such effects usually suppress the coherent singlet-triplet interconversion that underpins their metrological sensitivity. This raises fundamental questions: How close to quantum limits could SCRPs operate under noisy biological conditions? And could nature have optimized SCRPs in the open [20–23] to enable optimal magnetosensitivity?

Recent work comparing SCRPs models in terms of the quantum Cramér-Rao bound (QCRB) [24, 25], which sets a fundamental limit on parameter estimation precision [26, 27], showed a partial approach towards the QCRB in the limits of quantum system complexity, i.e. when increasing the number of hyperfine couplings towards biologically representative numbers. However, the precision fell short of that of the QCRB by more than an order of magnitude. In this letter, we demonstrate that intrinsic interrational motion can drive magnetosensing in SCRPs to over 90% of the quantum limit, achieving up to sub-degree angular precision, challenging the prevalent notion that environmental noise and molecular motion would preclude sensitivity near the quantum limit. Specifically, we consider driven radical-pair systems, motivated by prior findings showing how Landau-

Zener-Stückelberg-Majorana (LZSM) transitions [28] can enhance chemical signal contrast [29], with similarly periodic driving also having been shown to boost precision in quantum thermometry [30]. We establish quantum limits by considering the relationship between radical motion and the QCRB for  $\text{FAD}^{\bullet-}/\text{W}_C^{\bullet+}$  as a representative radical-pair in cryptochrome, with our results informing more broadly about systems subject to electron spin-spin interactions, such as EED and/or exchange couplings.

*Radical-Pair Model.*—We consider radical-pairs interacting with an external magnetic field and magnetic nuclei via Zeeman and hyperfine interactions, respectively. The time-independent part of the Hamiltonian defining these interactions is

$$\begin{aligned}\hat{H}_0 &= \hat{H}_{\text{Zeeman}} + \hat{H}_{\text{Hyperfine}} \\ &= \sum_i \vec{\omega}_i \cdot \hat{\mathbf{S}}_i + \sum_i \sum_j \hat{\mathbf{S}}_i \cdot \mathbf{A}_{i,j} \cdot \hat{\mathbf{I}}_{i,j},\end{aligned}\quad (1)$$

where the Larmor precession frequency  $\vec{\omega}_i = -\gamma_i \mathbf{B}$  is given by the product of the magnetic field  $\mathbf{B} = B_0(\sin \theta \cos \phi, \sin \theta \sin \phi, \cos \theta)$ , with  $B_0$  denoting the magnitude ( $\sim 50 \mu\text{T}$  for the geomagnetic field), and the electron gyromagnetic ratios. The electron spin in the  $i$ th radical is denoted  $\hat{\mathbf{S}}_i$ , whilst the nuclear spin  $\hat{\mathbf{I}}_{i,j}$  is coupled to the  $i$ th electron spin via hyperfine coupling tensors  $\mathbf{A}_{i,j}$ . Additionally, we introduce time-dependent dipolar and exchange interactions between electron spins and random-field relaxation (RFR). The time-dependent part of the Hamiltonian that defines these interactions is

$$\begin{aligned}\hat{H}_1(t) &= \hat{H}_{\text{Dipolar}}(t) + \hat{H}_{\text{Exchange}}(t) + \hat{H}_{\text{RFR}}(t) \\ &= \hat{\mathbf{S}}_1 \cdot \mathbf{D}(t) \cdot \hat{\mathbf{S}}_2 - 2J(t)\hat{\mathbf{S}}_1 \cdot \hat{\mathbf{S}}_2 \\ &\quad + \sum_{i=1,2} \sum_{j=x,y,z} \mathbf{b}_{i,j}(t) \cdot \hat{\mathbf{S}}_{i,j},\end{aligned}\quad (2)$$

where  $\mathbf{D}(t)$  is the electron-electron dipolar (EED) coupling tensor,  $J(t)$  is the exchange coupling, and  $\mathbf{b}_{i,j}(t)$  denotes uncorrelated magnetic field noise of equal strength across the three Cartesian coordinates. The EED tensor and exchange coupling are proportional to  $r^{-3}(t)$ , and  $\exp(-\beta r(t))$  with  $\beta = 1.4 \text{ \AA}^{-1}$  [31], respectively. Specific forms of the interrational modulation  $r(t)$ , including harmonically driven [29] and optimally controlled [29, 32] cases, are discussed in the Appendix, with parameters reported in the Supplemental Material (SM).

Following the photoinduced electron transfer reaction that forms the candidate magnetoreceptor  $\text{FAD}^{\bullet-}/\text{W}_C^{\bullet+}$ , the initial state is an electronic singlet state, given by a spin density operator  $\hat{\rho}(0) = \frac{\hat{P}_S}{Z}$ , where  $\hat{P}_S$  is the singlet projection operator and  $Z = Z_A Z_B$  denotes the dimension of the nuclear subspace associated with the two radicals. This initial state evolves under the total Hamiltonian  $\hat{H}(t) = \hat{H}_0 + \hat{H}_1(t)$  via the master equation  $\partial_t \hat{\rho}_\theta(t) = -i[\hat{H}(t), \hat{\rho}_\theta(t)] - \hat{K}(t)\hat{\rho}_\theta(t)$ , where,  $\hat{K}(t)$  is the reaction operator comprising the reaction rate for product formation  $k_f$  and time-dependent recombination  $k_b(t)$ ,  $[\cdot, \cdot]$  indicates the commutator, and  $\hat{\rho}_\theta = \hat{\rho}(t, \theta, \phi)$  signifies that the state acquires sensitivity to the magnetic field inclination through the Zeeman interaction. In this letter, we restrict to  $k_b(0) = k_f = 1 \mu\text{s}^{-1}$ , reflecting the asymmetry in the reaction channels from singlet and triplet states typically found in cryptochromes [10, 33]. From  $\hat{\rho}_\theta(t)$ , the singlet population can be calculated as  $p_S(t) = \text{Tr}[\hat{P}_S \hat{\rho}_\theta(t)]$ , with the singlet yield defined as

$$\Phi_S = \int_0^\infty k_b(t) p_S(t) dt. \quad (3)$$

From this the established relative anisotropy measure of sensitivity that quantifies the contrast in recombination yields over all magnetic-field directions is obtained by  $\Gamma = (\Phi_{S,\text{max}} - \Phi_{S,\text{min}})/\bar{\Phi}_S$  where  $\Phi_{S,\text{max}}$  and  $\Phi_{S,\text{min}}$  represent the maximum and minimum recombination yields and  $\bar{\Phi}_S$  indicates the mean recombination yield.

*Quantum Metrology.*—Following the framework established in [24] we define the probe state as the steady state  $\hat{\rho}_{\text{ss}}$  of continuous generation and recombination, evaluated from  $\hat{\rho}_\theta(t)$  with specific details provided in the Appendix. As the electron spins couple to the magnetic field via the Zeeman interaction, the electronic part of  $\hat{\rho}_{\text{ss}}$  encodes the intensity and directional dependence of the magnetic field. The quantum Fisher information (QFI) [34] and the associated quantum Cramér–Rao bound (QCRB) [25] constrain the maximal precision attainable in the statistical estimation of a parameter  $\vartheta$  from measurements on a quantum state  $\hat{\rho}_\vartheta$ . For an unbiased estimator based on  $N$  independent measurements, the bound is provided by  $\frac{1}{\delta^2 \vartheta} \leq N F_\vartheta \leq N \mathcal{F}_\vartheta$  where  $\delta^2 \vartheta$  represents the variance of the  $\vartheta$ -estimates,  $F(\vartheta)$  is the classical Fisher information (CFI) [35, 36] for any observable,  $\mathcal{F}(\vartheta)$  is the QFI. Specifically, the classical

Fisher information establishes the sensitivity of the state to a particular set of measurements and takes the form,

$$F_\vartheta = \sum_n p_{n,\vartheta} (\partial_\vartheta \ln p_{n,\vartheta})^2 = \sum_n \frac{(\partial_\vartheta p_{n,\vartheta})^2}{p_{n,\vartheta}}, \quad (4)$$

where we have used, and  $p_{n,\vartheta} = \text{Tr}[\hat{\rho}_\vartheta \hat{\Pi}_n]$  are the Born rule probabilities associated with the measurement element  $\hat{\Pi}_n$ , where  $\sum_n \hat{\Pi}_n = \hat{I}$  with  $\hat{I}$  denoting the identity operator, given that the state of the system before the measurement was  $\hat{\rho}_\vartheta$ . The QFI can be obtained by optimizing the CFI over all possible measurements. This framework can thus be used to analyze the quantum limit of precision in estimating a magnetic field parameter  $\vartheta = \theta$  as realizable in SCRPs, by choosing a set of measurements for the CFI  $\Pi_n \in \{\hat{P}_S, \hat{P}_T\}$ , where  $\hat{P}_S$  and  $\hat{P}_T = \hat{I} - \hat{P}_S$ , are the singlet and triplet projection operators, respectively. This represents measurements in the magnetosensitive basis associated with chemically distinguishable outcomes, for which spin-selective recombination reactions of the radical-pair are the only anticipated mechanism in natural systems. Specifically, the ratio  $F_\theta/\mathcal{F}_\theta$  can be used to assess the precision of singlet-triplet-based measurements in a SCRPs, where  $F_\theta/\mathcal{F}_\theta \leq 1$  represents the degree of approach to QCRB and a value of 1 represents its saturation.

*Noise and interrational modulation.*—We evaluate the approach to the QCRB for a simple driven radical-pair model comprising nucleus N5, representing the dominant hyperfine coupling of  $\text{FAD}^{\bullet-}/\text{W}_C^{\bullet+}$ . Fig. 1 shows the ratio of  $F_\theta/\mathcal{F}_\theta$ , which indicates how closely the system approaches the QCRB, for driving frequency  $\nu_d$  against exchange coupling  $J_0$ . Due to the approximate axial symmetry of the hyperfine interaction for this system [24], we scan over  $\theta$  and set  $\phi = 0$ . To evaluate how noise and interrational interactions influence metrological performance for the driven model, we consider three progressively complex scenarios in Fig. 1: (a) exchange only, neglecting EED interactions and relaxation, (b) inclusion of EED, and (c) inclusion of both EED and RFR (with relaxation rate  $\gamma = 1 \mu\text{s}^{-1}$ ). To maintain focus on regions of increased sensitivity, in panels (b) and (c), we restrict  $F_\theta/\mathcal{F}_\theta$  to points where the relative anisotropy  $\Gamma$  is maintained or improved relative to the undriven, exchange-interaction-free reference  $\Gamma(J_0 = 0, \nu_d = 0)$ . In panel (a), where the idealized absence of dipolar and relaxation effects leads to unrealistically high baseline sensitivities, we instead restrict  $F_\theta/\mathcal{F}_\theta$  to points where the relative anisotropy does not fall below 10% of the reference. This reflects the idea that a measurement, even if optimal, must induce a noticeable chemical change.

Interestingly, under moderate driving ( $1 \leq \nu_d \leq 100 \text{ MHz}$ ), the system can attain 96.4% saturation of the QCRB. Moreover, with the inclusion of EED and RFR, the optimization is generally more significant, especially in the frequency range of  $0 \leq \nu_d \leq 10 \text{ MHz}$ ,

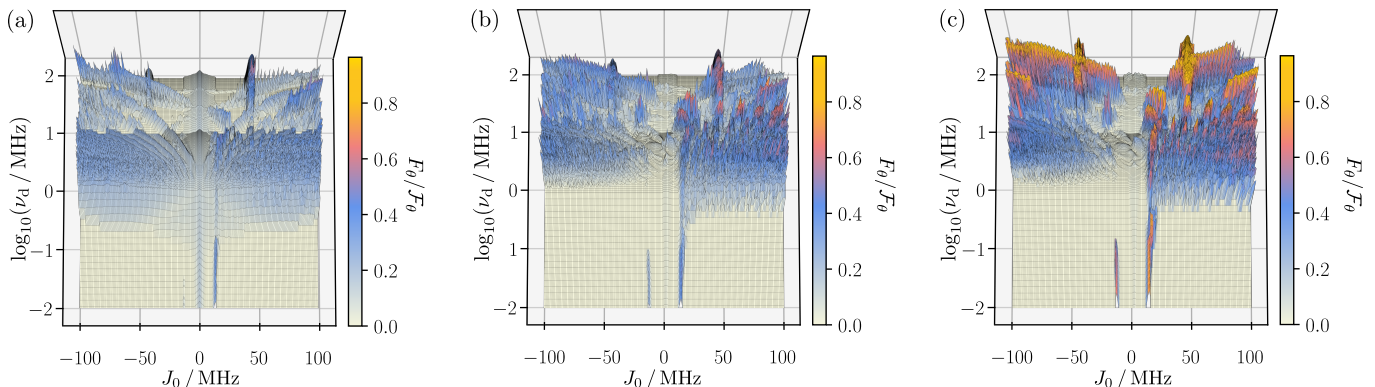


FIG. 1. Approach to the quantum Cramér-Rao bound (QCRB) under driven dynamics in a simple radical-pair model comprising the N5 nucleus, representing the dominant hyperfine coupling of  $\text{FAD}^{\bullet-}/\text{W}_C^{\bullet+}$ . The approach is assessed via the ratio of classical to quantum Fisher information  $F_\theta/\mathcal{F}_\theta$ , plotted as a function of  $209 \times 200$  combinations of driving frequencies  $\nu_d$  and exchange couplings  $J_0$  spanning  $0.01 \leq \nu_d \leq 100$  MHz and  $-100 \leq J_0/2\pi \leq 100$  MHz, respectively. Each point corresponds to the maximum ratio achieved over 180 magnetic field orientations ( $\theta \in [0, \pi]$  at fixed  $\phi = 0$ ). Panels show scenarios of increasing system complexity: (a) exchange only; (b) inclusion of electron-electron dipolar coupling (EED) interactions; (c) inclusion of both EED, and random-field noise (RFR). Driving enables up to 96.4% saturation of the QCRB, and as complexity is added, systems display more extensive approaches to the QCRB.

which was found to support relative anisotropy enhancements [29, 37]. Although absolute magnitudes inevitably decrease, they remain robust: the maximal QFI reaches  $N\mathcal{F}_\theta = 32.4$ , 5.40, & 0.153, and the CFI reaches  $NF_\theta = 1.22$ , 0.708, & 0.129, in the exchange only, with-EED, and with-RFR-and-EED scenarios, respectively. At these maximal values, the static system is vastly outperformed, with QFI smaller by two to three orders of magnitude, and CFI smaller by two to six orders of magnitude. This shows that driven interrational modulations not only optimize the system in approach to the QCRB but significantly increase the absolute performance by enhancing the magnitude of precision as compared to the static scenario. Additional simulations of QFI and CFI magnitudes and ratios can be found in the SM.

*Biologically motivated system.*—Moving toward a more biologically representative model of  $\text{FAD}^{\bullet-}/\text{W}_C^{\bullet+}$ , we include the N5 and N1 hyperfine couplings, each localized on a different radical, with EED and exchange interactions included. Fig. 2(a) shows the ratio of  $F_\theta/\mathcal{F}_\theta$  to indicate the approach to the QCRB, for driving frequency  $\nu_d$  against exchange coupling  $J_0$  within the range identified as beneficial in the N5-system. As axial symmetry is broken in this model system, we sampled over  $\theta$  &  $\phi$ .  $F_\theta/\mathcal{F}_\theta$  is displayed at all points, for which there is an improvement over the static reference in the magnitudes of relative anisotropy, CFI, and QFI. We evaluated all quantities over orientations to the magnetic field  $\theta$  and  $\phi$  and took the maximum as representative, as a particular scanning axis through varying reaction yields could be selected or have evolved to contain the maximal point, while qualitatively similar results emerge for the average, shown in the SM. In the Appendix, we provide further details on how this scheme can be viewed as a measure-

ment of the total electronic spin, with the CFI equivalent to the error in measuring the square of the total angular momentum  $\hat{S}^2$ , the relation to reaction yields, and evaluation of the QFI.

Close approaches to the QCRB are observed over a broad range of exchange coupling and driving frequencies. At the optimal point, where  $F_\theta/\mathcal{F}_\theta = 0.895$ , the singlet yield  $\Phi_S$  profile is plotted in Fig. 2(b) alongside its static counterpart. Driving significantly enhances both yield contrast and the relative anisotropy, increasing  $\Gamma$  from  $1.84 \times 10^{-4}$  in the static system to 0.093 under driving. Unlike the static case, where yield fluctuations obscure a scanning axis through  $\theta$  and  $\phi$ , the driven yield profile exhibits a clear high-yield and low-yield point, establishing a well-defined scanning axis. Taking the points of maximum and minimum  $\Phi_S$  and plotting the associated singlet probabilities  $p_S$  in Fig. 2(c), shows that the enhancement is due to the restoration of coherent singlet-triplet oscillations, driven at the modulation frequency. Although driving can generally break the field-inversion symmetry, we find the effect to be minor: at the closest approach to the QCRB the relative anisotropy differs by only 0.065% and the average yield by  $1.46 \times 10^{-4}\%$ , when comparing one hemisphere with the other, as shown in the SM. Finally, we note that the degree of approach to the QCRB from the inclusion of driving is broadly maintained on increasing in the number of hyperfine couplings from one to two; in the Appendix we show that this trend is maintained for four coupled nuclei.

*Precision under quantum control.*—Thus far, harmonic modulations of recombination, exchange and electron-electron dipolar interactions have been shown to enhance magnetic field sensing through improving yield contrast, the precision, and the approach to quantum limits as as-

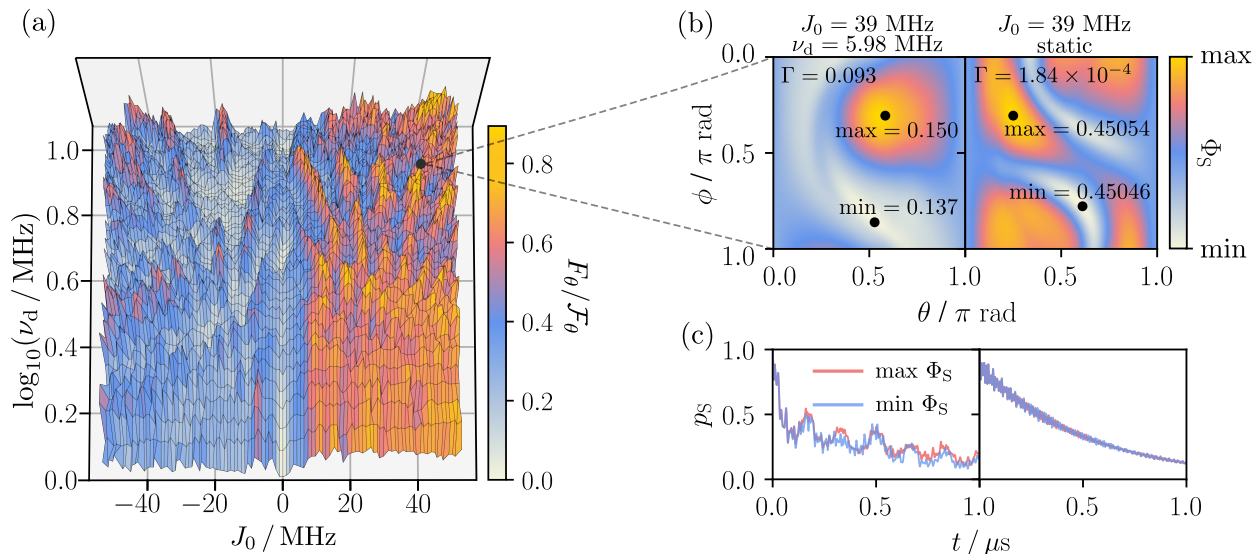


FIG. 2. Approach to the quantum Cramér-Rao bound (QCRB) under driven dynamics in a representative radical-pair model of  $\text{FAD}^{\bullet-}/\text{W}_C^{\bullet+}$  comprising N5 and N1 hyperfine couplings, electron-electron dipolar and exchange interactions. (a) The QCRB is assessed via the ratio of classical to quantum Fisher information  $F_\theta/\mathcal{F}_\theta$ , plotted as a function of 48  $\times$  100 combinations of driving frequencies  $\nu_d$  and exchange couplings  $J_0$  spanning  $1 \leq \nu_d \leq 10$  MHz and  $-50 \leq J_0/2\pi \leq 50$  MHz, respectively. Each point corresponds to the maximum value achieved over  $37 \times 37$  magnetic field orientations ( $\theta$  &  $\phi \in [0, \pi]$ ). (b) The singlet yield  $\Phi_S$  profile for the closest approach to the QCRB at  $F_\theta/\mathcal{F}_\theta = 0.895$  is shown and compared to the static system, with relative anisotropy  $\Gamma$  indicated. (c) Singlet probability  $p_S$  over time that gives rise to the maximum and minimum singlet yields. Overall, driving provides close approaches to the QCRB, providing a larger contrast in yield and better defined scanning axis, originating from a restoration of coherent oscillations in the singlet probability at the driving frequency.

essed by the CFI and the QCRB. To consider whether a more complex interrational modulation could achieve further improved results, we leverage optimal quantum control [32, 38–43], conditioned upon maximizing the yield contrast ( $\Phi_{S,\text{max}} - \Phi_{S,\text{min}}$ ) of the biologically representative  $\text{FAD}^{\bullet-}/\text{W}_C^{\bullet+}$  model, to derive optimized interrational fluctuations. The latter is then used to compare to the static and harmonically driven system in Fig. 3 by generating (a) the relative anisotropy ( $\Gamma$ ), (b) the CFI ( $NF_\theta$ ), (c) and the QFI ( $N\mathcal{F}_\theta$ ) plotted against exchange coupling. The control results exhibit a marked enhancement across the majority of  $J_0$  values, for relative anisotropy, CFI, and QFI, reaching as high as  $\Gamma = 0.863$ ,  $NF_\theta = 1.43$ , and  $N\mathcal{F}_\theta = 3.68$ . The harmonically driven system is generally lower, with maximum values at  $\Gamma = 0.161$ ,  $NF_\theta = 0.161$ , and  $N\mathcal{F}_\theta = 0.503$ , yet it still marks a significant improvement over the static system at  $\Gamma = 0.044$ ,  $NF_\theta = 0.036$ , and  $N\mathcal{F}_\theta = 0.064$ . With control, approaches to the QCRB as close as  $F_\theta/\mathcal{F}_\theta = 0.97$  can be reached. Translation of results into explicit angular precision estimates can be found in the Appendix, and further plots of the QCRB can be found in the SM.

*Discussion.*—Experiments *in vitro* suggest a photo-induced  $\text{FAD}^{\bullet-}/\text{W}_C^{\bullet+}$  radical-pair [44–50], generated via electron transfer from a tryptophan residue ( $\text{W}_C$ ) to a flavin adenine dinucleotide (FAD) cofactor, as a potential SCRPs underpinning a biochemical compass sensor. An alternative candidate,  $\text{FADH}^\bullet/\text{O}_2^{\bullet-}$ , formed in the

dark during flavin reoxidation with molecular oxygen, is also occasionally deliberated [51–57]. Both share the dilemma that, while simple models of their spin dynamics suggest their feasibility to underpin a compass in principle, models of realistic complexity accounting for effects of quantum noise predict only marginal sensitivity, casting doubts on their ability to provide an effective sensory modality. To resolve this, additional enhancement mechanisms have been proposed, including exchange/dipolar cancellation [58], three-radical mechanisms [59, 60], radical scavenging [61], relaxation-assisted mechanisms [62, 63], diffusive [64] and driven-radical motion [6, 29, 65], the quantum Zeno effect [66–68], and chirality-induced spin selectivity [69–71]. Various metrics, such as energy resolution limits [72], mutual information [73, 74], Wigner-Yanase skew information [75], and quantum Fisher information (QFI) [24, 76, 77], have been explored, relating the sensing performance to the number of magnetoreceptors, coherence, and measurement strategy.

Nevertheless, most studies of enhancement mechanisms focus on the chemical reaction yield contrast over magnetic field orientation, which does not directly establish whether the ultimate limits of quantum precision are approached, nor identify how high the ceiling of magnetometric performance goes. Our approach, on the other hand, provides more direct insight into how nature may have harnessed structural adaptations from biophysics

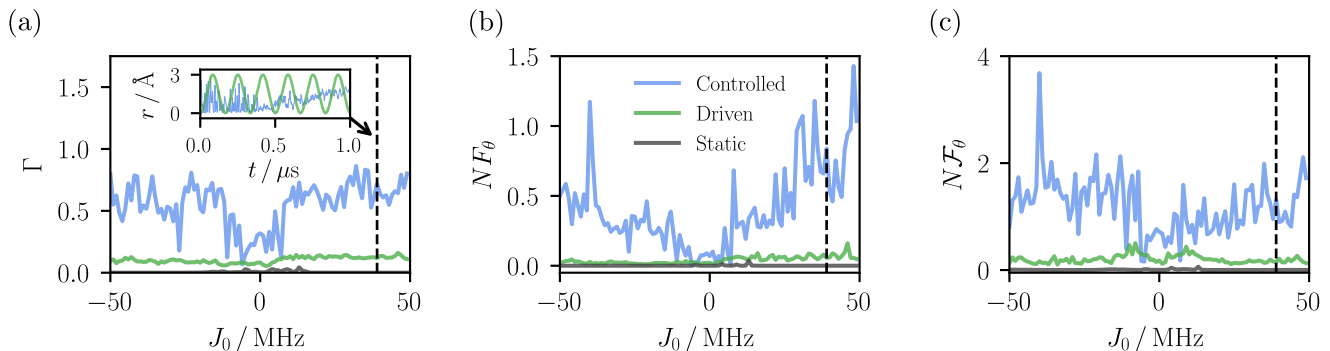


FIG. 3. Comparison of quantum-controlled interradical fluctuations that maximize yield contrast, harmonically driven fluctuations, and the static system. (a) Relative anisotropy ( $\Gamma$ ), with inset showing the modulated interradical distance for both control and driven cases at the optimal exchange coupling value  $J_0/2\pi = 39$  MHz. (b) Classical Fisher information ( $N\mathcal{F}_\theta$ ), and (c) quantum Fisher information ( $N\mathcal{F}_\theta$ ), calculated over  $37 \times 37$  combinations of  $\theta$  &  $\phi \in [0, \pi]$  across the exchange coupling range  $-50 \leq J_0/2\pi \leq 50$  MHz, with maximum values reported. Quantum-controlled fluctuations generate the strongest enhancements, followed by the driven system, both of which significantly outperform the static system.

to leverage environment-assisted quantum dynamics [78–81], principles of which could be exploited in tunable molecular quantum technologies [1, 4, 5] for information processing and metrology. We expect our results to generalize beyond  $\text{FAD}^{\bullet-}/\text{W}_\text{C}^{\bullet+}$  to radical systems in which modulations can arise naturally or can be engineered, with their underlying physical principles potentially also offering a route towards identifying biomimetic design principles for quantum sensing. Particularly promising are systems with reference-probe characteristics [82–85], such as  $\text{FADH}^{\bullet-}/\text{O}_2^{\bullet-}$  or the hypothetical  $\text{FAD}^{\bullet-}/\text{Z}^{\bullet}$  [82]. Future work could investigate structured modulations in molecular dynamics simulations, where periodic motion with frequency components in the beneficial 1–10 MHz range have indeed been recently observed [65], and explore whether alternative mechanisms, such as the quantum Zeno effect in tightly bound radicals [66], can similarly approach quantum-limited performance.

*Conclusion.*—We have shown that interradical modulations induced by molecular motion can push the angular precision in magnetic field sensing towards the quantum limit set by the quantum Cramér-Rao bound. Remarkably, realistic system complexities, including exchange and dipolar couplings, random field relaxation noise, and increased hyperfine couplings, were found to augment this. This originates from restored singlet-triplet coherence, driven by Landau-Zener-Stückelberg-Majorana transitions [28, 29] that increase the chemical yield contrast and both classical/quantum Fisher information. While even harmonic modulations are effective, modulations identified through quantum control [2, 29, 32, 86–88], and combining harmonic components at 1–10 MHz with components resonant with hyperfine splittings, enable substantially greater precision. Such modulations, which may have emerged in cryptochromes over their 541–1000 million years of evolution from DNA

photolyases [20–23], reduce the untenable angular errors predicted for the static system (exceeding  $100^\circ$ ) to within the biological functional window of degrees [74, 89–91], and offer scope for engineering sub-degree improvements beyond what nature may have achieved.

The authors acknowledge support from the Office of Naval Research Global (ONR-G Award Number N62909-21-1-2018), the Engineering and Physical Sciences Research Council (EPSRC grants EP/V047175/1 and EP/X027376/1) and the Biotechnology and Biological Sciences Research Council (BBSRC grants BB/Y514147/1, BB/Y51312X/1). JG is supported by a Leverhulme Trust Research Project Grant (RPG-2023-177). The authors further acknowledge the use of the University of Exeter High Performance Computing Facility. For the purpose of open access, the authors have applied a Creative Commons Attribution (CC BY) license to any Author Accepted Manuscript version arising from this submission.

- 
- [1] N. Lin *et al.*, Molecular engineering of emissive molecular qubits based on spin-correlated radical pairs, *J. Am. Chem. Soc.* **147**, 11062 (2025).
  - [2] P. J. Hore, Spin control of hybrid quantum-dot-based radical pairs, *Nat. Mater.* **24**, 171 (2025).
  - [3] M. Liu *et al.*, Coherent manipulation of photochemical spin-triplet formation in quantum dot-molecule hybrids, *Nat. Mater.* **24**, 260 (2025).
  - [4] T. Mani, Molecular qubits based on photogenerated spin-correlated radical pairs for quantum sensing, *Chem. Phys. Rev.* **3**, 021301 (2022).
  - [5] C.-J. Yu, S. Von Kugelgen, D. W. Laorenza, and D. E. Freedman, A molecular approach to quantum sensing, *ACS Cent. Sci.* **7**, 712 (2021).
  - [6] M. Hamada, T. Iwata, M. Fuki, H. Kandori, S. We-

- ber, and Y. Kobori, Orientations and water dynamics of photoinduced secondary charge-separated states for magnetoreception by cryptochrome, *Commun Chem* **4**, 141 (2021).
- [7] R. Bittl and K. Schulten, Biradical spin dynamics with distance-dependent exchange interaction and electron transfer efficiency, *Chem. Phys. Lett.* **173**, 387 (1990).
- [8] J. Xu *et al.*, Magnetic sensitivity of cryptochrome 4 from a migratory songbird, *Nature* **594**, 535 (2021).
- [9] R. Wiltschko and W. Wiltschko, Magnetoreception in birds, *Journal of The Royal Society Interface* **16**, 20190295 (2019).
- [10] P. J. Hore and H. Mouritsen, The radical-pair mechanism of magnetoreception, *Annu. Rev. Biophys.* **45**, 299 (2016).
- [11] T. Ritz, S. Adem, and K. Schulten, A model for photoreceptor-based magnetoreception in birds, *Biophys. J.* **78**, 707 (2000).
- [12] A. Sotoodehfar *et al.*, Quantum theory of a potential biological magnetic field sensor: radical pair mechanism in flavin adenine dinucleotide biradicals, *Comput. Struct. Biotechnol. J.* **26**, 70 (2024).
- [13] G. Grüning, L. Gerhards, S. Y. Wong, D. R. Kattnig, and I. A. Solov'yov, The effect of spin relaxation on magnetic compass sensitivity in ercry4a, *ChemPhysChem* **25**, e202400129 (2024).
- [14] N. S. Babcock and D. R. Kattnig, Electron–electron dipolar interaction poses a challenge to the radical pair mechanism of magnetoreception, *J. Phys. Chem. Lett.* **11**, 2414 (2020).
- [15] D. R. Kattnig, I. A. Solov'yov, and P. J. Hore, Electron spin relaxation in cryptochrome-based magnetoreception, *Phys. Chem. Chem. Phys.* **18**, 12443 (2016).
- [16] A. V. Bogdanov, B. Y. Mladenova Kattnig, A. K. Vorobiev, G. Grampp, and A. I. Kokorin, Rotational dynamics of nitroxide biradical in room-temperature ionic liquids measured by quantitative simulation of epr spectra, *J. Phys. Chem. B* **124**, 11007 (2020).
- [17] K. Sato *et al.*, Trityl-aryl-nitroxide-based genuinely g-engineered biradicals, as studied by dynamic nuclear polarization, multifrequency esr/endor, arbitrary wave generator pulse microwave waveform spectroscopy, and quantum chemical calculations, *J. Phys. Chem. A* **123**, 7507 (2019).
- [18] H. M. Hoang, V. T. B. Pham, G. Grampp, and D. R. Kattnig, Magnetic field-sensitive radical pair dynamics in polymethylene ether-bridged donor–acceptor systems, *ACS Omega* **3**, 10296 (2018), pMID: 30198006.
- [19] S. Nakazawa *et al.*, A synthetic two-spin quantum bit: g-engineered exchange-coupled biradical designed for controlled-not gate operations, *Angew. Chem. Int. Ed.* **51**, 9860 (2012).
- [20] R. Bartölke, H. Behrmann, K. Görtemaker, C. Yee, J. Xu, E. Behrmann, and K. W. Koch, The secrets of cryptochromes: Photoreceptors, clock proteins, and magnetic sensors, *Neuroforum* **27**, 151 (2021).
- [21] Q. Mei and V. Dvornyk, Evolutionary history of the photolyase/cryptochrome superfamily in eukaryotes, *PLoS One* **10**, e0135940 (2015).
- [22] M. Liedvogel and H. Mouritsen, Cryptochromes—a potential magnetoreceptor: What do we know and what do we want to know?, *J. R. Soc. Interface* **7**, S147 (2010).
- [23] A. R. Cashmore, J. A. Jarillo, Y. J. Wu, and D. Liu, Cryptochromes: blue light receptors for plants and animals, *Science* **284**, 760 (1999).
- [24] L. D. Smith, J. Glatthard, F. T. Chowdhury, and D. R. Kattnig, On the optimality of the radical-pair quantum compass, *Quantum. Sci. Technol.* **9**, 035041 (2024).
- [25] A. Holevo, *Probabilistic and statistical aspects of quantum theory* (Edizioni della Normale Pisa, 2011).
- [26] V. Montenegro, C. Mukhopadhyay, R. Yousefjani, S. Sarkar, U. Mishra, M. G. Paris, and A. Bayat, Quantum metrology and sensing with many-body systems, *Phys. Rep.* **1134**, 1 (2025).
- [27] F. J. Headley, A. Belenchia, M. Paternostro, and D. Braun, Quantum metrology of newton’s constant with levitated mechanical systems, arXiv:2503.16215 10.48550/arXiv.2503.16215 (2025).
- [28] O. V. Ivakhnenko, S. N. Shevchenko, and F. Nori, Nonadiabatic landau–zener–stüeckelberg–majorana transitions, dynamics, and interference, *Physics Reports* **995**, 1 (2023).
- [29] L. D. Smith, F. T. Chowdhury, I. Peasgood, N. Dawkins, and D. R. Kattnig, Driven radical motion enhances cryptochrome magnetoreception: Toward live quantum sensing, *J. Phys. Chem. Lett.* **13**, 10500 (2022).
- [30] J. Glatthard and L. A. Correa, Bending the rules of low-temperature thermometry with periodic driving, *Quantum* **6**, 705 (2022).
- [31] C. C. Moser, J. M. Keske, K. Warncke, R. S. Farid, and P. L. Dutton, Nature of biological electron transfer, *Nature* **355**, 796 (1992).
- [32] F. T. Chowdhury, M. C. Denton, D. C. Bonser, and D. R. Kattnig, Quantum control of radical-pair dynamics beyond time-local optimization, *PRX Quantum* **5**, 020303 (2024).
- [33] K. Maeda, A. J. Robinson, K. B. Henbest, H. J. Hogben, T. Biskup, M. Ahmad, E. Schleicher, S. Weber, C. R. Timmel, and P. J. Hore, Magnetically sensitive light-induced reactions in cryptochrome are consistent with its proposed role as a magnetoreceptor, *Proceedings of the National Academy of Sciences* **109**, 4774 (2012), <https://www.pnas.org/doi/pdf/10.1073/pnas.1118959109>.
- [34] S. L. Braunstein and C. M. Caves, Statistical distance and the geometry of quantum states, *Phys. Rev. Lett.* **72**, 3439 (1994).
- [35] R. A. Fisher, Theory of Statistical Estimation, *Math. Proc. Cambridge Philos. Soc.* **22**, 700 (1925), publisher: Cambridge University Press.
- [36] M. G. Paris, Quantum estimation for quantum technology, *Int. J. Quantum Inf.* **7**, 125 (2009).
- [37] H. M. Hoang, T. B. V. Pham, G. Grampp, and D. R. Kattnig, Exciplexes versus loose ion pairs: How does the driving force impact the initial product ratio of photoinduced charge separation reactions?, *J. Phys. Chem. Lett.* **5**, 3188 (2014), pMID: 25243054.
- [38] T. Rehmert, M. J. Zawierucha, K. Dietze, P. O. Schmidt, and F. Wolf, Quantum logic control of a transition metal ion, *Phys. Rev. Lett.* **134**, 113201 (2025).
- [39] A. N. Poddubny, K. Winkler, B. A. Stickler, U. Delić, M. Aspelmeyer, and A. V. Zasedatelev, Nonequilibrium entanglement between levitated masses under optimal control, arXiv:2408.06251 10.48550/arXiv.2408.06251 (2024).
- [40] M. P. Woods, Quantum frequential computing: a quadratic run time advantage for all algorithms, arXiv:2403.02389 10.48550/arXiv.2403.02389 (2024).
- [41] N. Pancotti, M. Scandi, M. T. Mitchison, and

- M. Perarnau-Llobet, Speed-ups to isothermality: Enhanced quantum thermal machines through control of the system-bath coupling, *Phys. Rev. X* **10**, 031015 (2020).
- [42] Z. Zimborás, R. Zeier, T. Schulte-Herbrüggen, and D. Burgarth, Symmetry criteria for quantum simulability of effective interactions, *Phys. Rev. A* **92**, 042309 (2015).
- [43] J. Cai, G. G. Guerreschi, and H. J. Briegel, Quantum control and entanglement in a chemical compass, *Phys. Rev. Lett.* **104**, 220502 (2010).
- [44] J. L. Ramsay, F. Schuhmann, I. A. Solov'yov, and D. R. Kattinig, Cryptochrome magnetoreception: Time course of photoactivation from non-equilibrium coarse-grained molecular dynamics, *Comput. Struct. Biotechnol. J.* **26**, 58 (2024).
- [45] A. Frederiksen, C. Langebrake, M. Hanić, G. Manthey, H. Mouritsen, M. Liedvogel, and I. A. Solov'yov, Mutational Study of the Tryptophan Tetrad Important for Electron Transfer in European Robin Cryptochrome 4a, *ACS Omega* **8**, 26425 (2023).
- [46] S. Y. Wong, Y. Wei, H. Mouritsen, I. A. Solov'yov, and P. J. Hore, Cryptochrome magnetoreception: four tryptophans could be better than three, *J. R. Soc. Interface* **18**, 20210601 (2021).
- [47] D. R. Kattinig, E. W. Evans, V. Déjean, C. A. Dodson, M. I. Wallace, S. R. Mackenzie, C. R. Timmel, and P. J. Hore, Chemical amplification of magnetic field effects relevant to avian magnetoreception, *Nat. Chem* **8**, 384 (2016).
- [48] D. Nohr, S. Franz, R. Rodriguez, B. Paulus, L.-O. Essen, S. Weber, and E. Schleicher, Extended Electron-Transfer in Animal Cryptochromes Mediated by a Tetrad of Aromatic Amino Acids, *Biophys. J.* **111**, 301 (2016).
- [49] P. Müller, J. Yamamoto, R. Martin, S. Iwai, and K. Brettel, Discovery and functional analysis of a 4th electron-transferring tryptophan conserved exclusively in animal cryptochromes and (6-4) photolyases, *Chem. Commun.* **51**, 15502 (2015).
- [50] B. Giovani, M. Byrdin, M. Ahmad, and K. Brettel, Light-induced electron transfer in a cryptochrome blue-light photoreceptor, *Nat. Struct. Mol. Biol.* **10**, 489 (2003).
- [51] J. Deviers, F. Cailliez, A. de la Lande, and D. R. Kattinig, Avian cryptochrome 4 binds superoxide, *Comput. Struct. Biotechnol. J.* **26**, 11 (2024).
- [52] K. M. Salerno, J. Domenico, N. Q. Le, K. Balakrishnan, R. J. McQuillen, C. D. Stiles, I. A. Solov'yov, and C. F. Martino, Long-Time Oxygen and Superoxide Localization in *Arabidopsis thaliana* Cryptochrome, *J. Chem. Inf. Model.* **63**, 6756 (2023).
- [53] L.-D. Arthaut, N. Jourdan, A. Mteyrek, M. Procopio, M. El-Esawi, A. d'Harlingue, P.-E. Bouchet, J. Wiczak, T. Ritz, A. Klarsfeld, S. Birman, R. J. Usselman, U. Hoecker, C. F. Martino, and M. Ahmad, Blue-light induced accumulation of reactive oxygen species is a consequence of the *Drosophila* cryptochrome photocycle, *PLOS One* **12**, e0171836 (2017).
- [54] L. J. G. W. van Wilderen, G. Silkstone, M. Mason, J. J. van Thor, and M. T. Wilson, Kinetic studies on the oxidation of semiquinone and hydroquinone forms of *Arabidopsis* cryptochrome by molecular oxygen, *FEBS Open Bio* **5**, 885 (2015).
- [55] P. Müller and M. Ahmad, Light-activated cryptochrome reacts with molecular oxygen to form a flavin-superoxide radical pair consistent with magnetoreception, *J. Biol. Chem.* **286**, 21033 (2011).
- [56] T. Ritz, R. Wiltschko, P. J. Hore, C. T. Rodgers, K. Stapput, P. Thalau, C. R. Timmel, and W. Wiltschko, Magnetic compass of birds is based on a molecule with optimal directional sensitivity, *Biophys. J.* **96**, 3451 (2009).
- [57] V. Massey, Activation of molecular oxygen by flavins and flavoproteins., *J. Biol. Chem.* **269**, 22459 (1994).
- [58] O. Efimova and P. J. Hore, Role of Exchange and Dipolar Interactions in the Radical Pair Model of the Avian Magnetic Compass, *Biophys. J.* **94**, 1565 (2008).
- [59] D. R. Kattinig, Radical-pair-based magnetoreception amplified by radical scavenging: Resilience to spin relaxation, *J. Phys. Chem. B* **121**, 10215 (2017).
- [60] R. H. Keens, S. Bedkihal, and D. R. Kattinig, Magnetosensitivity in dipolarly coupled three-Spin systems, *Phys. Rev. Lett.* **121**, 096001 (2018).
- [61] D. R. Kattinig and P. J. Hore, The sensitivity of a radical pair compass magnetoreceptor can be significantly amplified by radical scavengers, *Sci. Rep.* **7**, 1 (2017), publisher: Nature Publishing Group.
- [62] J. Luo, Sensitivity enhancement of radical-pair magnetoreceptors as a result of spin decoherence, *J. Chem. Phys.* **160**, 074306 (2024).
- [63] D. R. Kattinig, J. K. Sowa, I. A. Solov'yov, and P. J. Hore, Electron spin relaxation can enhance the performance of a cryptochrome-based magnetic compass sensor, *New J. Phys.* **18**, 063007 (2016).
- [64] J. L. Ramsay and D. R. Kattinig, Magnetoreception in cryptochrome enabled by one-dimensional radical motion, *AVS Quantum Sci.* **5**, 22601 (2023).
- [65] P. L. Benjamin, L. Gerhards, I. A. Solov'yov, and P. J. Hore, Magnetosensitivity of model flavin-tryptophan radical pairs in a dynamic protein environment, *J. Phys. Chem. B* **0**, null (0).
- [66] M. C. J. Denton, L. D. Smith, W. Xu, J. Pugsley, A. Toghill, and D. R. Kattinig, Magnetosensitivity of tightly bound radical pairs in cryptochrome is enabled by the quantum Zeno effect, *Nat. Commun.* **15**, 10823 (2024).
- [67] D. Burgarth, P. Facchi, H. Nakazato, S. Pascazio, and K. Yuasa, Quantum Zeno Dynamics from General Quantum Operations, *Quantum* **4**, 289 (2020).
- [68] A. T. Dellis and I. K. Kominis, The quantum Zeno effect immunizes the avian compass against the deleterious effects of exchange and dipolar interactions, *Biosyst.* **107**, 153 (2012).
- [69] L. D. Smith, S. Tallapudi, M. C. J. Denton, and D. R. Kattinig, Chirality-bolstered quantum zeno effect enhances radical pair-based magnetoreception, [arXiv:2505.01519](https://arxiv.org/abs/2505.01519) [10.48550/arXiv.2505.01519](https://arxiv.org/abs/2505.01519) (2025).
- [70] Y. Tiwari and V. S. Poonia, Role of chiral-induced spin selectivity in the radical pair mechanism of avian magnetoreception, *Phys. Rev. E* **106**, 064409 (2022).
- [71] J. Luo and P. J. Hore, Chiral-induced spin selectivity in the formation and recombination of radical pairs: cryptochrome magnetoreception and epr detection, *New J. Phys.* **23**, 043032 (2021).
- [72] I. K. Kominis and E. Gkoudinakis, Approaching the quantum limit of energy resolution in animal magnetoreception, *PRX Life* **3**, 013004 (2025).
- [73] Y. Ren, H. G. Hiscock, and P. Hore, Angular precision of radical pair compass magnetoreceptors, *Biophysical Journal* **120**, 547 (2021).
- [74] H. G. Hiscock, T. W. Hiscock, D. R. Kattinig, T. Scrivener, A. M. Lewis, D. E. Manolopoulos, and P. J.

- Hore, Navigating at night: fundamental limits on the sensitivity of radical pair magnetoreception under dim light, *Quarterly Reviews of Biophysics* **52**, e9 (2019).
- [75] I. K. Kominis, Physiological search for quantum biological sensing effects based on the wigner–yanase connection between coherence and uncertainty, *Advanced Quantum Technologies* **8**, 2300292 (2023).
- [76] K. M. Vitalis and I. K. Kominis, Quantum-limited biochemical magnetometers designed using the fisher information and quantum reaction control, *Phys. Rev. A* **95**, 032129 (2017).
- [77] L. S. Guo, B. M. Xu, J. Zou, and B. Shao, Quantifying magnetic sensitivity of radical pair based compass by quantum fisher information, *Sci. Rep.* **7**, 1 (2017).
- [78] Z. Wang and L. Jiang, Passive environment-assisted quantum communication with gkp states, *Phys. Rev. X* **15**, 021003 (2025).
- [79] W. Xu, A. A. Bagrov, F. T. Chowdhury, L. D. Smith, D. R. Kattnig, H. J. Kappen, and M. I. Katsnelson, Fröhlich versus bose-einstein condensation in pumped bosonic systems, *Phys. Rev. Res.* **7**, 023111 (2025).
- [80] J. S. Peter, R. Holzinger, S. Ostermann, and S. F. Yelin, Examining the quantum signatures of optimal excitation energy transfer, *Phys. Rev. Res.* **6**, 033252 (2024).
- [81] A. Dodin and P. Brumer, Noise-induced coherence in molecular processes, *J. Phys. B: At. Mol. Opt. Phys* **54**, 223001 (2022).
- [82] A. A. Lee, J. C. S. Lau, H. J. Hogben, T. Biskup, D. R. Kattnig, and P. J. Hore, Alternative radical pairs for cryptochrome-based magnetoreception, *J. R. Soc. Interface* **11**, 20131063 (2014).
- [83] J. Cai, F. Caruso, and M. B. Plenio, Quantum limits for the magnetic sensitivity of a chemical compass, *Phys. Rev. A* **85**, 040304 (2012).
- [84] T. Ritz, M. Ahmad, H. Mouritsen, R. Wiltschko, and W. Wiltschko, Photoreceptor-based magnetoreception: Optimal design of receptor molecules, cells, and neuronal processing, *J. R. Soc. Interface* **7**, S135 (2010).
- [85] C. R. Timmel, F. Cintolesi, B. Brocklehurst, and P. J. Hore, Model calculations of magnetic field effects on the recombination reactions of radicals with anisotropic hyperfine interactions, *Chem. Phys. Lett.* **334**, 387 (2001).
- [86] K. Meng, L. Nie, J. Berger, N. R. von Grafenstein, C. Einholz, R. Rizzato, E. Schleicher, and D. B. Bucher, Optically detected and radio wave-controlled spin chemistry in cryptochrome, [arXiv:2504.16566](https://arxiv.org/abs/2504.16566) 10.48550/arXiv.2504.16566 (2025).
- [87] A. Tateno, H. Nagashima, and K. Maeda, Effect of frequency chirp on rydmr spectrum in awg-rydmr system at low magnetic field, *Chem. Phys. Lett.* **864**, 141905 (2025).
- [88] U. G. Abdulla, J. Rodrigues, P. Jimenez, C. Zhen, and C. Martino, Bang-bang optimal control in coherent spin dynamics of radical pairs in quantum biology, *Quantum. Sci. Technol.* **9**, 045022 (2024).
- [89] X. Chen, H. Liu, and J. Cai, Identifying a possible mechanism for the quantum needle in chemical magnetoreception, *Phys. Rev. A* **110**, 042220 (2024).
- [90] S. Schwarze, F. Steenken, N. Thiele, D. Kobylkov, N. Lefeldt, D. Dreyer, N.-L. Schneider, and H. Mouritsen, Migratory blackcaps can use their magnetic compass at 5 degrees inclination, but are completely random at 0 degrees inclination, *Scientific Reports* **6**, 33805 (2016).
- [91] S. Åkesson, J. Morin, R. Muheim, and U. Ottosson, Avian orientation at steep angles of inclination: experiments with migratory white-crowned sparrows at the magnetic north pole, *Proc. R. Soc. Lond., Ser. B, Biol. Sci.* **268**, 1907 (2001).
- [92] G. Grüning, S. Y. Wong, L. Gerhards, F. Schuhmann, D. R. Kattnig, P. J. Hore, and I. A. Solov'yov, Effects of dynamical degrees of freedom on magnetic compass sensitivity: A comparison of plant and avian cryptochromes, *J. Am. Chem. Soc.* **144**, 22902 (2022).
- [93] D. Šafránek, Simple expression for the quantum Fisher information matrix, *Phys. Rev. A* **97**, 042322 (2018).
- [94] A. Dey, M. T. Johnsson, and D. Burgarth, Qualitative differences in the robust controllability of model two-qubit systems, [arXiv:2502.04102](https://arxiv.org/abs/2502.04102) 10.48550/arXiv.2502.04102 (2025).
- [95] N. Khaneja, T. Reiss, C. Kehlet, T. Schulte-Herbrüggen, and S. J. Glaser, Optimal control of coupled spin dynamics: design of NMR pulse sequences by gradient ascent algorithms, *J. Magn. Reson.* **172**, 296 (2005).
- [96] S. Campbell *et al.*, Roadmap on quantum thermodynamics, [arXiv:2504.20145](https://arxiv.org/abs/2504.20145) (2025).

## APPENDIX

*Harmonically driven interrational motion.*— Following the approach in [29], we introduce radical motion

$$r(t) = \frac{\Delta_d}{2}[1 - \cos(2\pi\nu_d t)] + r_0, \quad (\text{A1})$$

where  $\nu_d$  is the driving frequency and the driving amplitude is set to  $\Delta_d = 3 \text{ \AA}$ , as it was previously found to produce significant sensitivity enhancements while constituting a relatively modest motion.  $r_0 = 17.2 \text{ \AA}$  specifies the interrational distance of the static  $\text{FAD}^{\bullet-}/\text{W}_C^{\bullet+}$  radical-pair [92]. This radical motion modulates the dipolar coupling as

$$\hat{H}(t)_{\text{Dipolar}} = -d(r(t)) \left[ 3(\hat{\mathbf{S}}_1 \cdot \mathbf{u})(\hat{\mathbf{S}}_2 \cdot \mathbf{u}) - \hat{\mathbf{S}}_1 \cdot \hat{\mathbf{S}}_2 \right], \quad (\text{A2})$$

where  $d(r(t)) \equiv \mu_0 g_e^2 \mu_B^2 / 4\pi r(t)^3 > 0$ , with  $r \equiv |\mathbf{r}|$  and constants taking their usual definitions, and  $\mathbf{u} = \mathbf{r}/r$ . The recombination [29] is modulated as

$$k_b(t) = k_{b_0} \exp[-\beta(r(t) - r_0)], \quad (\text{A3})$$

The exchange interaction is modulated in the same functional form as

$$\hat{H}(t)_{\text{Exchange}} = -2J(t)\hat{\mathbf{S}}_1 \cdot \hat{\mathbf{S}}_2, \quad (\text{A4})$$

with  $J(t) = J_0 \exp[-\beta(r(t) - r_0)]$ . Together with Eqs. 1 and 2 these define

$$\hat{H}_{\text{eff}}(t) = \hat{H}(t) - i \left( \frac{k_b(t)}{2} \hat{P}_S + \frac{k_f}{2} \hat{I} \right). \quad (\text{A5})$$

Using above and following [24], we define the probe state as the radical-pair in a steady-state of continuous generation and recombination as  $\hat{\rho}_{\text{ss}} = \frac{k_0 c}{Z} \tilde{G}(s=0) \hat{P}_S$ , with  $k_0$  denoting the generation rate,  $c$  the (constant) concentration of cryptochrome in the resting state, and  $\tilde{G}(s)$  is the Laplace transform of  $\hat{G}(t)$ .

*Explicit CFI and QFI formulations.*— Extending the results of [24] to a system under time-dependent interrational motion, the CFI using Eq. 4 with measurement elements  $\hat{\Pi}_n \in \{\hat{P}_S, \hat{P}_T\}$  takes the form

$$\begin{aligned} F_\theta &= \frac{(\partial_\theta \text{Tr}[\hat{P}_S \hat{\sigma}_{\text{ss}}])^2}{\text{Tr}[\hat{P}_S \hat{\sigma}_{\text{ss}}]} + \frac{(\partial_\theta \text{Tr}[(\hat{I} - \hat{P}_S) \hat{\sigma}_{\text{ss}}])^2}{\text{Tr}[(\hat{I} - \hat{P}_S) \hat{\sigma}_{\text{ss}}]} \\ &= \frac{(\partial_\theta \Theta_S)^2}{\Theta_S(1 - \Theta_S)} \end{aligned} \quad (\text{A6})$$

where  $\hat{\sigma}_{\text{ss}}$  is the normalized spin density operator and  $\Theta_S = \text{Tr}[\hat{P}_S \hat{\sigma}_{\text{ss}}]$  represents the the expectation value of the conditional singlet probability, which is the probability of finding the system in the singlet state, conditioned on its survival. Following the derivation in [24], it follows

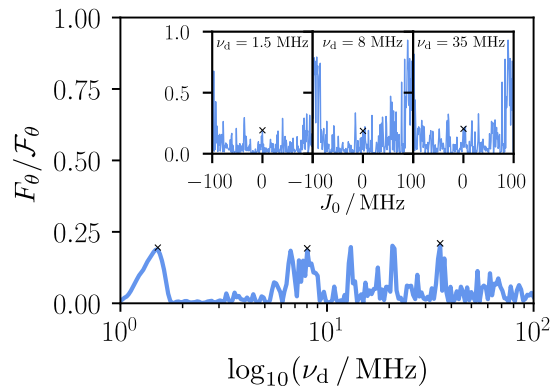


FIG. A1. Robustness of approach to the quantum Cramér-Rao bound (QCRB) under driven dynamics of  $\text{FAD}^{\bullet-}/\text{W}_C^{\bullet+}$  with four hyperfine couplings (N5 and N10 in FAD; N1 and H1 in Trp) electron-electron dipolar and exchange interactions. Approach is assessed by  $F_\theta/\mathcal{F}_\theta$  for the case of  $J_0/2\pi = 0 \text{ MHz}$  with 200 driving frequencies in the range  $1 \leq \nu_d \leq 100 \text{ MHz}$ , while insets extend the exchange coupling to 200 values in the range  $-100 \leq J_0/2\pi \leq 100 \text{ MHz}$  for select driving frequencies  $\nu_d = 1.5, 8, \& 35 \text{ MHz}$ .  $F_\theta/\mathcal{F}_\theta$  is evaluated for orientations maximizing and minimizing yield difference in the static case. This shows that approaches to the QCRB are maintained on increase of hyperfine complexity.

that  $1/\Delta^2\theta = NF_\theta$  still holds when considering the error associated with measuring observable  $\hat{O} = \hat{S}^2$  through  $N$  independent measurements. However, we note that  $\Theta_S$  differs from the singlet yield  $\Phi_S$  due to the time-dependent nature of the recombination rate constant, and the relation to singlet yield is only reclaimed in the limit of the static system (up to normalization).

To obtain the QFI [36], we note that  $\partial_\theta p_{n,\theta} = \text{Tr}[\partial_\theta \hat{\rho}_\theta \hat{\Pi}_n] = \text{Tr}[\hat{\rho}_\theta \hat{\Pi}_n \hat{L}_\theta]$ , where  $\hat{L}_\theta$  is the symmetric logarithmic derivative. Maximizing the CFI over  $\{\hat{\Pi}_n\}$  gives  $\text{Tr}(\hat{L}_\theta^2 \hat{\rho}_\theta) = \mathcal{F}_\theta$ . In the basis that diagonalizes  $\hat{\rho}_\theta$ , and using the spectral decomposition  $\hat{\rho}_\theta = \sum_i p_i |\psi_i\rangle\langle\psi_i|$ , we obtain

$$\mathcal{F}_\theta = 2 \sum_{p_i + p_j \neq 0} \frac{1}{p_i + p_j} |\langle\psi_i|\partial_\theta \hat{\rho}_\theta|\psi_j\rangle|^2. \quad (\text{A7})$$

Alternative approaches to compute the QFI are possible if  $\hat{\rho}_\theta$  is invertible [93].

*Robustness to hyperfine complexity.*— While it is known that the magnitude of relative anisotropy decreases [92] as the number of hyperfine coupled nuclei is increased in  $\text{FAD}^{\bullet-}/\text{W}_C^{\bullet+}$ , we show that the factor of enhancement from driving persists [29]. To see how robust the approach to the QCRB is to system complexity in the driven system, we increase the number of hyperfine couplings in the radical-pair to four (two in each radical), adding the next most relevant hyperfine couplings N10 and H1. Fig. A1 shows the ratio of  $F_\theta/\mathcal{F}_\theta$ ,

over a wide range of 200 driving frequencies in the range  $1 \leq \nu_d \leq 100$  MHz in the presence of EED interactions with  $J_0/2\pi = 0$  MHz, where insets show select driving values of  $\nu_d = 1.5, 8, \& 35$  MHz where  $F_\theta/\mathcal{F}_\theta$  peaks, extended over the range  $-100 \leq J_0/2\pi \leq 100$  MHz. Here, only orientations of  $\theta$  and  $\phi$  that maximize and minimize the yield difference of the static system are scanned, to allow the dense and wide parameter analysis over exchange coupling and driving frequency. Despite this minimal scan, close approaches to saturating the QCRB are reached (up to  $F_\theta/\mathcal{F}_\theta = 0.930$ ). In the SM we demonstrate similar degrees of optimality of a reduced scan of the two-nucleus radical-pair, suggesting that the approach to the QCRB from interradical fluctuations is maintained as hyperfine couplings are added.

*Optimal quantum control.*— We discretize our control functions into piecewise-constant segments, as standard in gradient-based approaches [94, 95]. The total Hamiltonian including the drift and control parts, with  $u_j$  constant during each interval, is

$$\hat{H}_{\text{Total}}(u_j) = \hat{H}_{\text{Drift}} + f_A(u_j)\hat{H}_A + f_B(u_j)\hat{H}_B, \quad (\text{A8})$$

where  $f_A$  considers the exchange interaction with an exponential dependence (as in Eq. A4), and  $f_B$  considers the dipolar with an inverse cubic dependence (as in Eq. A2). Following the approach from [32], the controls are optimized to maximize the difference in yields:  $\Phi_{S,\text{max}} - \Phi_{S,\text{min}}$ , with min and max in this case referring to the magnetic field orientations of the minimal and maximal yield respectively in the absence of the controlled distance fluctuations. In practice, the resulting optimization problem  $\max_{\mathbf{u}} J(\mathbf{u})$  is numerically solved by transforming into a minimization form, with  $\mathbf{u}$  mapped to displacement of the radicals from their position in the crystal structure, while enforcing boundedness and smoothness. We use 1000 controls of 1 ns each, whereby the maximal displacement is bound to 3 Å, ensuring physical feasibility of controls.

*Angular precision magnitudes.*—To translate our findings into explicit estimates of angular precision, we use the energy resolution limit [72] to estimate the minimum number of magnetoreceptors required for sensing. For radical-pair lifetimes in the range 1–10  $\mu\text{s}$ , this corresponds to an effective number of active magnetoreceptors between  $N = 2 \times 10^6$  and  $N = 2 \times 10^5$ , in line with previous estimates [74]. We then calculate the total classical Fisher information and use the Cramér-Rao bound to estimate the angular precision  $\Delta\theta = \sqrt{NF_\theta}$  obtainable from singlet and triplet measurements in the representative  $\text{FAD}^{\bullet-}/\text{W}_C^{\bullet+}$  system. Using this approach, we find angular precisions ranging from  $0.101^\circ$ – $0.319^\circ$  under harmonic driving, and  $0.034^\circ$ – $0.107^\circ$  with quantum-control-optimized interradical perturbations. For the static case, optimal precision ranges from  $0.214^\circ$ – $0.675^\circ$ , however, for the representative scenario of  $J_0/2\pi = 0$  MHz, the performance deteriorates to as low as  $9.11^\circ$  –  $28.8^\circ$ , corresponding to  $NF_\theta = 1.98 \times 10^{-5}$ .

By analyzing how precision degrades with increasing hyperfine complexity (e.g.,  $NF_\theta = 0.029$ , corresponding to  $0.238^\circ$ – $0.752^\circ$  at four couplings), we extrapolate that in more biologically realistic regimes [96] with tens of hyperfine couplings, the CFI under harmonic driving ( $NF_\theta \sim 10^{-3}$ – $10^{-4}$ ) would yield angular precision on the order of a few degrees. Although RFR noise would lead to further degradation by roughly an order of magnitude in the CFI, structured perturbations, as in the quantum-controlled system, could more than compensate for this. In contrast, a static system with similar complexity performs far worse: previous analysis shows  $NF_\theta \sim 1 \times 10^{-7}$  even without RFR, such that formally the angular precision amounts to  $128 - 405^\circ$ . Finally, using the QFI, the fundamental bounds on angular precision are estimated as  $0.007^\circ - 0.0225^\circ$  for the idealized single nucleus model (neglecting EED), and  $0.021^\circ - 0.067^\circ$  for the representative two-spin  $\text{FAD}^{\bullet-}/\text{W}_C^{\bullet+}$  system.